Recent developments in optical fibre sensing using fibre Bragg gratings

G. P. Brady, K. Kalli, D. J. Webb, D. A. Jackson,
L. Zhang[†] and I. Bennion[†]

Applied Optics Group, Physics Laboratory, University of Kent at Canterbury, Canterbury, Kent, CT2 7NR, UK.
[†]Photonics Research Group, Department of Electronic Engineering, Aston University, Birmingham, B4 7ET, UK.

ABSTRACT

We report on recent work on sensing using in-fibre Bragg gratings carried out in our laboratory. Firstly, an alternative method of discriminating between temperature and strain effects using a conventionally written, in-fibre Bragg grating is presented. The technique uses wavelength information from the first and second diffraction orders of the grating element to determine the wavelength dependent strain and temperature coefficients, from which independent temperature and strain measurements can be made. Secondly, we describe an all-fibre, passive scheme for making extended range interferometric measurements based on the dual wavelength technique. A coherence tuned interferometer network is illuminated with a single superfluorescent fibre source at 1.55mm and the two wavelengths are synthesised at the output by means of chirped fibre Bragg gratings.

Keywords: Optical fibre sensing, Bragg grating, temperature, strain, low coherence, dual wavelength.

1. INTRODUCTION

Bragg grating sensors (BGSs) have generated great interest in recent years because of their potential use in a wide range of applications, particularly in monitoring the structural integrity of buildings, bridges and advanced composite materials. BGSs form an integral part of the optical fibre structure, being written intracore whilst the fibre is manufactured[1], and provide absolute wavelength encoding of information that is independent of overall system light levels, but dependent upon strain and temperature effects acting upon the sensor. In this paper we report on two pieces of research related to Bragg grating sensors that have been carried out within our laboratories.

2. DISCRIMINATION BETWEEN THE EFFECTS OF TEMPERATURE AND STRAIN

As mentioned above, BGSs are sensitive to both temperature and strain and a single measurement of the Bragg wavelength shift cannot distinguish between their effects. Such an ability is of primary importance if BGSs are to realise their considerable potential in real-world applications. Several discriminating techniques have been demonstrated in recent years; these include the use of a second grating element encapsulated in a different material and placed in-line to the first grating to provide temperature compensating data[2] and most recently the use of two superimposed fibre grating sensors[3]. Here, we demonstrate an alternative technique that uses the primary and second order diffraction from a single, interferometrically written BGS to decouple the effects of temperature and strain[4]. Our experimental data, justifying the feasibilty of this approach are accompanied by a treatment of how errors in the measurement of a BGS wavelength change map to errors in the decoupled strain and temperature data.

2.1 Second order grating diffraction

The grating recording process is nonlinear, with continued exposure resulting in saturation of the index perturbation. One may therefore anticipate the existence of higher order grating reflections at roughly integer multiples of the primary reflected optical frequency, i.e. 1/integer multiples of the incident wavelength. Of course, the strength of these higher order reflections is determined by the magnitude of their respective Fourier coefficients which now describe the index perturbation; for conventionally written, medium reflectivity gratings the second order signal will be very small. Xie *et al* [5] first observed second order diffraction from Bragg gratings written within germanosilicate fibres. Their best results were obtained when the second order wavelength, at 734nm, approached the LP_{11} cut-off wavelength, 0.74mm; thus at the second order wavelength the fibre was virtually single mode. The primary wavelength was written at 1451nm. The ratio of

 0-8194-2227-4/96/$6.00

the two wavelengths was not exactly two due to material and waveguide dispersion. However, they did not observe any second order reflection from gratings written in fibre similar to that used in our work, where we operate in the few-moded regime.

2.2 Dual wavelength technique

The dual wavelength approach[6] for discriminating between changes in temperature ΔT and strain $\Delta\varepsilon$ assumes that these perturbations are linearly superimposed, with a negligible cross term $\Delta\varepsilon\Delta T$. A single measurement of the wavelength shift recovered from a perturbed BGS is thus given by,

$$\Delta\lambda(\varepsilon,T) = \Delta\lambda_\varepsilon + \Delta\lambda_T = K_\varepsilon\Delta\varepsilon + K_T\Delta T, \quad (1)$$

where $\Delta\lambda_\varepsilon$ and $\Delta\lambda_T$ are the temperature and strain induced wavelength shifts and K_ε and K_T are the strain and temperature coefficients, respectively. Any wavelength dependence arises from the photoelastic and thermo-optic coefficients, hence a grating illuminated with two distinct wavelengths and exposed to the same level of temperature and/or strain perturbation will produce different wavelength shifts. One may construct a matrix equation relating the temperature and strain coefficients at the two different wavelengths of illumination:

$$\begin{bmatrix} \Delta\lambda_1 \\ \Delta\lambda_2 \end{bmatrix} = \begin{bmatrix} K_{\varepsilon 1} & K_{T1} \\ K_{\varepsilon 2} & K_{T2} \end{bmatrix} \begin{bmatrix} \Delta\varepsilon \\ \Delta T \end{bmatrix}, \quad (2)$$

where the suffixes 1 and 2 refer to the two different wavelengths. Once the elements of the 2×2 matrix are determined by independent measurement of the Bragg wavelength change with strain and temperature at the two wavelengths of interest, inversion of the matrix can be used to determine the absolute temperature and strain information from measurements of the shifts at wavelengths 1 and 2. This technique is limited by the conditioning of the matrix inversion[3]; in particular the following condition must be satisfied,

$$\frac{K_{\varepsilon 1}}{K_{\varepsilon 2}} \neq \frac{K_{T1}}{K_{T2}}. \quad (3)$$

In the experiments that follow we use a Bragg grating written in standard telecommunications fibre, having a primary reflecting wavelength of 1561nm. The transmission profile of the grating is shown in Figure 1.

2.3 Experimental procedure for measuring strain and temperature at the second harmonic wavelength

Calculations incorporating the effects of material and waveguide dispersion gave an estimate of the second order Bragg reflection between 785-789nm and so a single mode laser diode (Mitsubishi ML4102) operating at 789nm with an output power of 1.5mW (at 25°C) was used for these experiments. The laser was made wavelength tunable by heating or cooling the case. The change in peak wavelength with temperature was measured using an optical spectrum analyser consisting of a miniature bulk diffraction grating and CCD array coupled to a digitizing oscilloscope. The current driving the laser diode was set to 46.5mA (the manufacturer's specified operating point) and the laser's change in wavelength was monitored as the case temperature dropped from 27.0°C to 23.5°C, from which the wavelength-to-temperature coefficient of the laser diode was calculated to be 0.0603±0.0026nm/°C.

2.4 Measurement of the strain coefficient at the second harmonic wavelength

The experimental configuration is shown in Figure 2. The fibre grating was mounted between two translation stages, separated by a distance of 44cm, thus allowing for direct straining of the grating element. To enable heating of the grating it was placed inside an insulated oven. The fibre ends of the coupler and grating fibre were angle polished at 20° to minimize any Fresnel back reflections into the system; thus any backreflected light could be attributed to the grating being wavelength matched to the source. The dynamic range of the signal recovery was enhanced by applying a small amplitude

current modulation of 0.5mA at a frequency of 45kHz to the laser injection current. The modulation current was chosen to be sufficiently small to prevent mode hopping of the laser emission spectrum and the frequency modulation produced was negligible compared to the grating bandwidth. Any signal reflected from the grating would therefore be amplitude modulated allowing a signal to be easily detected using a photodetector coupled to an HP 3561A dynamic signal analyser.

Illumination of the grating at 21.6°C and for a bias current of 46.5mA produced a strong 45kHz signal at a calculated wavelength of 788.8nm. This is an approximately 8nm difference from the simple assumption that the second harmonic occurs for a wavelength ratio of two. To test the validity of the experimental set-up, the fibre was heated with a powerful hot air blower at points A, B, C and on the grating itself. Continued heating throughout the fibre network produced minimal variation of the recovered signal, whereas an impulse of thermal energy on the grating caused the signal to fluctuate wildly before returning to the same stable signal level. Thus we could be sure that the detected signal was from the grating and not from a Fresnel reflection elsewhere. From the data obtained, we estimated the reflectivity of the grating at ~789nm to be 0.1%. It should be noted that the grating was two-moded at the wavelength of illumination, however, this did not prove at all problematic in achieving a strong lower order mode reflection from the grating. During the experiment it became apparent that there were four principle reflecting modes attributed to the grating, possibly resulting from reflections of the LP_{01} and LP_{11} spatial modes. The strongest reflection was always chosen for these measurements.

A known strain was applied to the grating using the micrometer translation stage so that the reflecting wavelength of the grating could be controlled. The laser diode was heated to 26.8°C and the grating was strained until the grating wavelength coincided with that of laser emission producing a strong peak on the signal analyser. The source was allowed to slowly cool down from 26.8°C to 21.6°C. As the laser diode wavelength decreased the strain on the grating was slowly released to track this change whilst maintaining the signal on the dynamic signal analyzer, Figure 3. From this data, and incorporating the wavelength to temperature coefficient measured in 2.3 above, the strain coefficient of the Bragg grating at ~789nm, $K_{\varepsilon 2}$, was calculated to be (0.603±0.026)nm/mε. The experiment was repeated several times giving very similar results. The measured value is in good agreement with that reported in reference 3 of 0.59nm/me measured at 850nm for a first order Bragg reflection in 800nm fibre.

2.5 Measurement of the temperature coefficient at the second harmonic wavelength

To measure the temperature coefficient of the BGS, the air in the oven was heated to in excess of 65°C and then allowed to cool. A thermocouple was used to measure the change in air temperature. The cooling cycle was slow (15 minutes to cool to 30°C) and hence the temperature of the grating was taken to be the same as that of the air in the oven given the small thermal mass of the fibre. The laser diode was kept at a constant temperature of 21.6°C with a steady bias current of 46.5mA, so that it emitted at a constant 788.8nm. Again a current modulation of amplitude 0.5mA at 45kHz was applied to the laser diode to allow signal recovery via the dynamic signal analyser.

The initial heating caused the secondary reflecting wavelength of the grating to increase to a certain value before slowly decreasing on the cooling cycle. To maintain a signal from the grating on the dynamic signal analyser a known strain was applied to the grating as it is cooled. Hence it was possible to recover data of applied strain to the grating versus temperature of the grating, i.e. the ratio of the strain and temperature coefficients, see Figure 4. It should be pointed out that if there was an appreciable cross term between temperature and strain, $\Delta\varepsilon\Delta T$, the graph would display significant nonlinearity; the data recovered is highly linear and we can therefore deduce that our initial assumptions for the validity of the inversion method hold, at least to within the strain and temperature measurement ranges used. From the graph we could calculate the second harmonic temperature coefficient, K_{T2}, to be $(6.604 \pm 0.031)\times10^{-3}$nm/°C.

2.6 Experimental procedure for measuring strain and temperature at the primary Bragg wavelength

The temperature and strain coefficients at 1561nm, corresponding to the primary reflecting wavelength of the in-fibre grating, were measured using the system shown in Figure 5. An erbium doped superfluorescent fibre source provided a high power output and a broad range of wavelengths (1530-1563nm) to illuminate the system. The signal reflected from the grating was incident upon a tunable Fabry-Perot (FP) filter, which was used to track any change in the grating wavelength in response to applied strain or temperature. The same precautions preventing backreflections through the fibre network were taken as specified in the previous sections.

A low frequency dither of 300Hz was applied to the FP filter to increase the sensitivity in tracking the signal reflected by the grating. As the grating was strained the reflected Bragg wavelength increased so the FP filter was tuned so that a maximum signal was recovered by the dynamic signal analyser. From this experiment, the primary wavelength strain coefficient was measured to be (1.203±0.017) nm/mε. The temperature coefficient was measured using the same oven arrangement as earlier. As the grating cooled the FP filter was again tuned so that a maximum signal was detected by the dynamic signal analyser. This experiment resulted in a measurement of $(11.877\pm0.181)\times10^{-3}$ nm/°C for the primary wavelength temperature coefficient.

2.7 Validity of the technique

We may now compare the values of the strain and temperature coefficients at the second harmonic wavelength with those at the primary wavelength. To summerise, the temperature and strain coefficients have been measured as,

$$\begin{aligned} K_{\varepsilon 1} &= (1.203 \pm 0.017) \times 10^{-3} \text{ nm/me} \\ K_{\varepsilon 2} &= (0.603 \pm 0.026) \times 10^{-3} \text{ nm/me} \\ K_{T1} &= (11.877 \pm 0.181) \times 10^{-3} \text{ nm/°C} \\ K_{T2} &= (6.604 \pm 0.031) \times 10^{-3} \text{ nm/°C} \end{aligned} \tag{4}$$

The ratios in equation (3) are given by,

$$\frac{K_{\varepsilon 1}}{K_{\varepsilon 2}} = 1.995 \pm 0.059 \qquad \frac{K_{T1}}{K_{T2}} = 1.798 \pm 0.062 \tag{5}$$

These differ by an amount greater than the errors arising from the experimental measurements and the method is therefore validated.

2.8 Relationship between errors in the wavelength measurements and errors in strain and temperature

Assuming that the coefficients for temperature and strain are well known, it is useful to obtain a measure of the error in temperature and strain after the matrix inversion that results from an uncertainty in the wavelength measurement. Any errors in the first and second harmonic wavelength measurements, λ_1 and λ_2, will produce errors in the measurement of strain and temperature. To gauge their significance, the mapping of wavelength space to strain-temperature space must be considered. Suppose the wavelength measurements have an error of "a" for λ_1 and "b" for λ_2 and that a and b are uncorrelated. The uncertainty in wavelength space will generally transform to an ellipse in strain-temperature space, see Figure 6. The maximum errors in strain, $\Delta\varepsilon_{max}$, and temperature, ΔT_{max}, can be calculated from this. Translating wavelength space so the wavelengths λ_1 and λ_2 are at the origin gives the error ellipse as

$$\frac{\Delta\lambda_1^2}{a^2} + \frac{\Delta\lambda_2^2}{b^2} = 1 , \tag{6}$$

where $\Delta\lambda_1$ and $\Delta\lambda_2$ are the errors in λ_1 and λ_2, respectively. This can be represented in matrix form as

$$\begin{bmatrix} \Delta\lambda_1 & \Delta\lambda_2 \end{bmatrix} \begin{bmatrix} \frac{1}{a^2} & 0 \\ 0 & \frac{1}{b^2} \end{bmatrix} \begin{bmatrix} \Delta\lambda_1 \\ \Delta\lambda_2 \end{bmatrix} = 1 . \tag{7}$$

Combining (7) and (2) leads to

$$\left(\frac{K_{T_1}^2}{a^2}+\frac{K_{T_2}^2}{b^2}\right)\Delta T^2+2\left(\frac{K_{\varepsilon_1}K_{T_1}}{a^2}+\frac{K_{\varepsilon_2}K_{T_2}}{b^2}\right)\Delta\varepsilon\Delta T+\left(\frac{K_{\varepsilon_1}^2}{a^2}+\frac{K_{\varepsilon_2}^2}{b^2}\right)\Delta\varepsilon^2=1 \tag{8}$$

This corresponds to an ellipse where the major and minor axes are not generally parallel to the strain or temperature axes. The maximum error in strain, $\Delta\varepsilon_{max}$, and temperature, ΔT_{max}, occur when the conditions

$$\left(\frac{d(\Delta\varepsilon)}{d(\Delta T)}\right)=0 \quad \text{and} \quad \left(\frac{d(\Delta T)}{d(\Delta\varepsilon)}\right)=0 \tag{9}$$

are respectively met. These conditions lead to the following expressions for the maximum errors:

$$\Delta\varepsilon_{max}=\pm\left|\left(\frac{K_{\varepsilon_1}^2}{a^2}+\frac{K_{\varepsilon_2}^2}{b^2}\right)-\frac{\left(\frac{K_{\varepsilon_1}K_{T_1}}{a^2}+\frac{K_{\varepsilon_2}K_{T_2}}{b^2}\right)^2}{\left(\frac{K_{T_1}^2}{a^2}+\frac{K_{T_2}^2}{b^2}\right)}\right|^{-\frac{1}{2}} \quad \Delta T_{max}=\pm\left|\left(\frac{K_{T_1}^2}{a^2}+\frac{K_{T_2}^2}{b^2}\right)-\frac{\left(\frac{K_{\varepsilon_1}K_{T_1}}{a^2}+\frac{K_{\varepsilon_2}K_{T_2}}{b^2}\right)^2}{\left(\frac{K_{\varepsilon_1}^2}{a^2}+\frac{K_{\varepsilon_2}^2}{b^2}\right)}\right|^{-\frac{1}{2}} \tag{10}$$

Putting the values for the coefficients of our grating into equations (10) and assuming that the wavelength measurement resolution is the same for both wavelengths gives the strain and temperature errors per pm error in the wavelength measurement as,

$$\Delta\varepsilon_{max}=\pm 17.4\ m\varepsilon/pm \qquad \Delta T_{max}=\pm 1.72\ °C/pm \tag{11}$$

This compares with strain and temperature errors of ±12 mε/pm and ±1.3 °C/pm arrived at by using the strain and temperature coefficients measured by Xu *et al*[3] for two superimposed gratings. This makes our approach appear quite attractive given the simplicity of using a single grating, whilst both techniques would require a near identical means of measuring the wavelength shifts at the two different wavelengths.

Kersey *et al*[7] have demonstrated a Bragg grating strain sensor with high resolution interferometric wavelength shift detection having a wavelength resolution of 1.2×10^{-12}m. Using this value for wavelength resolution, the errors in temperature and strain using the above approach would be ±2.1°C and ±21mε.

3. SYNTHESISED DUAL WAVELENGTH TECHNIQUE

When interferometric sensors are used to sense quasi-static measurands, their unambiguous range is limited by the repetitive nature of the interferometric transfer function to a change in optical path difference of one wavelength. For such systems, there have been a number of approaches to increase the unambiguous sensing range, based on polarimetric[8], white-light (coherence-tuned)[9] and dual wavelength interferometry[10,11]. The last technique is considered highly attractive allowing for relatively simple phase interrogation of the interferometer system using two discrete and closely spaced wavelengths. This approach allows for high resolution phase shift detection at either wavelength with the ability to sense absolutely over the unambiguous range, which can correspond to more than 100 wavelengths. For the technique to be practically useful one requires two highly stable sources.

Rather than using two discrete sources, the two wavelengths can be synthesised from a single broadband source using appropriate filters. For example, Kersey *et al*[12] have demonstrated the use of two intra-core narrow band Bragg gratings to provide the selection of two wavelength components having a separation of ~2.5nm. Dual wavelengths for use in

a coherence tuned syatem can also be synthesised with a single broadband source and a single broadband wavelength filter, the transmitted and reflected light being incident on two separate detectors[11]. Coherence tuning allows for the sensing interferometer to remain entirely passive with any active components located in the receiving interferometer and the absolute value of the measurand is recoverable on "switch-on". Furthermore, coherence tuned systems typically require a small optical path difference in the sensing interferometer, and thus do not place any great restraint on the source stability. In this paper we describe a variation on this coherence tuned, dual wavelength approach and interrogate a Fizeau cavity sensor with a Mach Zehnder interferometer entirely in-fibre, passively and using a single broadband superfluorescent fibre source to illuminate the system, the dual wavelengths being synthesised using chirped fibre Bragg gratings.

3.1 Experimental arrangement

The experimental system, shown in Figure 7, comprised of a remotely deployable Fizeau air path cavity sensor in series with an unbalanced fibre Mach-Zehnder interferometer. One fibre arm of the Mach-Zehnder interferometer incorporated a piezoelectric transducer (PZT) cylinder around which was wrapped 3m of fibre, which permitted electrical modulation of the interferometer's optical path difference. The system was illuminated with an erbium doped fibre superfluorescent source (SFS). The SFS provided approximately 100μW between 1530-1560nm, coupled with good spectral stability with respect to temperature (typically 5ppm/°C[13]). The pumping diode current was set to a level that allowed for two equal amplitude, broadband spectral features to be emitted from the SFS. The average wavelengths of these spectral lobes were measured to be 1534.8nm and 1541.4nm. The coherence lengths of the individual lobes were ~780μm and ~400μm, respectively.

The MZI had an optical path imbalance of 1500μm which exceeded the coherence length of the SFS. The path matching condition necessary for interference effects to be observed required that the unbalanced MZI had an approximately equal optical path difference to the Fizeau cavity (to within the coherence length of the SFS). Hence the Fizeau cavity provided optical path length compensation for a portion of the incident power such that interference fringes were observed for the composite system. The combined interferometer output was amplitude divided at a 3dB coupler and was incident on two identical chirped Bragg gratings of bandwidth 5nm and reflectivity ~85%; these were spliced in-line to improve the reflectivity. The gratings reflected the spectral peak centred around 1534.8nm and transmitted that centred around 1541.4nm, thus synthesising two broadband sources, which were detected by separate InGaAs photodiodes. The wavelength output from either detector provided high resolution (milli-rad) phase information, whilst a comparison of the two outputs gave extended range information. The transmission and reflection response of the chirped gratings is shown in Figure 8.

We used pseudo-heterodyne processing to recover the phase shift information at each wavelength by applying a 125Hz serrodyne modulation signal to the fibre MZI, with the amplitude adjusted to drive the coherence tuned interferometers over one fringe of their cycle. This provided two electrical carriers that were phase modulated by the test signal applied to the mirror of the Fizeau cavity, demodulation being carried out using lock-in amplifiers.

3.2 Results

The emission spectrum of the erbium doped SFFL is shown in Figure 9, together with the spectrum of light transmitted or reflected by the chirped Bragg gratings. The spectra were measured by splicing the gratings via a coupler to the SFFL and monitoring the transmitted or reflected light using an optical spectrum analyser (reflected light was monitored via the coupler). The effective wavelength, λ_{eff}, using the wavelengths 1534.8nm and 1541.4nm was calculated to be 358μm.

To demonstrate the variation in the phase difference between the two outputs, the Mach-Zehnder interferometer arm was not modulated and the mirror of the Fizeau cavity was swept linearly over a large, undetermined range. Figure 10 shows the raw demultiplexed fringes obtained from the detector. From an expanded version of the recovered data we determined that a phase difference of π radians occurred after 88 fringes ±1 fringe, thus the total unambiguous range of the differential output ($\pm\pi$) corresponding to ± 88 normal interferometric fringes at 1541.4nm resulted in an effective wavelength of 271μm. To monitor the single wavelength phase output of the Fizeau cavity, its mirror was changed for another mounted on a PZT with a controllable movement range that was swept over a range of 60μm (the limit of its

movement), i.e. a Fizeau cavity optical path difference of 120μm. Figure 11 shows the outputs obtained from the lock-in amplifiers monitoring the outputs at 1534.8nm and 1541.4nm. Figure 12 shows the differential output, this corresponds to an effective path difference of 268μm, this agrees with the experimental value derived from Figure 10 to within two interferometric fringes. Thus the unambiguous range has been extended by a factor of 174. The resolution of the system at one wavelength was also measured and found to be 1nm (minimum detectable phase of ~4 mrad) when normalised to a 1Hz bandwidth.

3.3 Wavelength Stability of the Technique

A key factor in a system such as this is its sensitivity to temperature variations, which may affect either the source profile or the grating centre wavelength. A drift in either may affect the values of the mean synthesised wavelengths. Our modelling of the effect of temperature on the grating centre wavelength suggests that a 1°C rise in temperature results in a shift in the mean wavelengths of 1.8×10^{-3}nm. By way of a comparison, if two narrow band gratings are used to synthesise the sources for a dual wavlength system[12], the corresponding value is 1.3×10^{-2}nm, showing that our approach offers an advantage in this area.

The temperature coefficient of erbium doped fibre is typically 5ppm/°C[13]. A temperature change in the source of 1.7°C will produce similar changes in transmitted and reflected mean wavelengths to a 1°C change in the grating temperature.

4. CONCLUSION

We have described the results of two research projects involving Bragg grating sensors. Data has been presented demonstrating the feasibility of using a medium reflectivity, conventionally written BGS for the simultaneous measurement of temperature and strain. The potential of this technique is clear, offering a useful advantage over the superimposed grating method as the scheme is suitable for use with gratings written during the fibre manufacturing process. A novel extended range interferometric system with good temperature stability has been described, using a Bragg grating to synthesise a dual wavelength source from the output of an erbium doped fibre superfluorescent source.

5. REFERENCES

1. C. G. Askins et al. "Stepped-wavelength optical-fiber Bragg grating arrays fabricated in line on a draw tower". *Opt. Lett.* Vol. 19, No. 2, pp. 147-149, 1994.
2. W. W. Morey et al. "Evaluation of a fiber Bragg grating hydrostatic pressure sensor". *Proc. OFS 8*, Monterey, USA, Postdeadline Paper PD-4.4, 1992.
3. M. G. Xu et al. "Discrimination between strain and temperature effects using dual-wavelength fibre grating sensors". *Elec. Lett.* Vol. 30, No. 13, pp. 1085-1087, 1994.
4. K. Kalli et al. "Possible approach for the simultaneous measurement of temperature and strain via first and second order diffraction from Bragg grating sensors". OFS '94, Glasgow. Postdeadline paper.
5. W. X. Xie et al. "Second order diffraction efficiency of Bragg gratings written within germanosilicate fibres". *Opt. Comm.* Vol. 101, No. 1,2, pp. 85-91, 1993.
6. F. Farahi et al. "Simultaneous measurement of temperature and strain: cross-sensitivity considerations". *J. Lightwave Tech.* Vol. 8, No. 2, pp. 138-142, 1990.
7. A. D. Kersey et al. "Fiber-optic Bragg grating strain sensor with drift-compensated high-resolution interferometric wavelength-shift detection". *Opt. Lett.* Vol. 18, No. 1, pp. 72-74, 1993.
8. P. Akhavan Leilabady, J. D. C. Jones, M. Corke and D. A. Jackson, "A dual interferometer implemented in parallel on a single birefringent monomode optical fibre", Journ. Phys. E. Vol. 19, (1986), pp. 143-146.
9. T. Bosselmann and R. Ulrich, "High-accuracy position-sensing with fiber-coupled white-light interferometry", Proc. 2nd int. conf. on optical fibre sensors (VDE Verlag, Stuttgart), 5th-7th Sept. (1984).
10. A. D. Kersey and A. Dandridge, "Dual-wavelength approach to interferometric sensing", Proc. Soc. Photo-Opt. Instrum. Eng., Vol. 798, Fiber Optic Sensors II, (1987), pp. 176-181.
11. D. J. Webb, J. D. C. Jones and D. A. Jackson, "Extended-range interferometry using a coherence-tuned, synthesised dual-wavelength technique with multimode fibre links", Electron. Lett. Vol. 24, No. 18, (1988), pp. 1173-1175.

12. A. D. Kersey and T. A. Berkoff, "Dual wavelength fibre interferometer with wavelength selection via fibre Bragg grating elements", Electron. Lett. Vol. 28, No. 28, (1992), pp. 1215-1216.
13. P. F. Wysocki, M. J. F. Digonnet and B. Y. Kim, "Wavelength stability of a high-output, broadband, Er-doped superfluorescent fiber source pumped near 980nm", Opt. Lett. Vol. 16, No. 12, (1991), pp. 961-963.

6. FIGURES

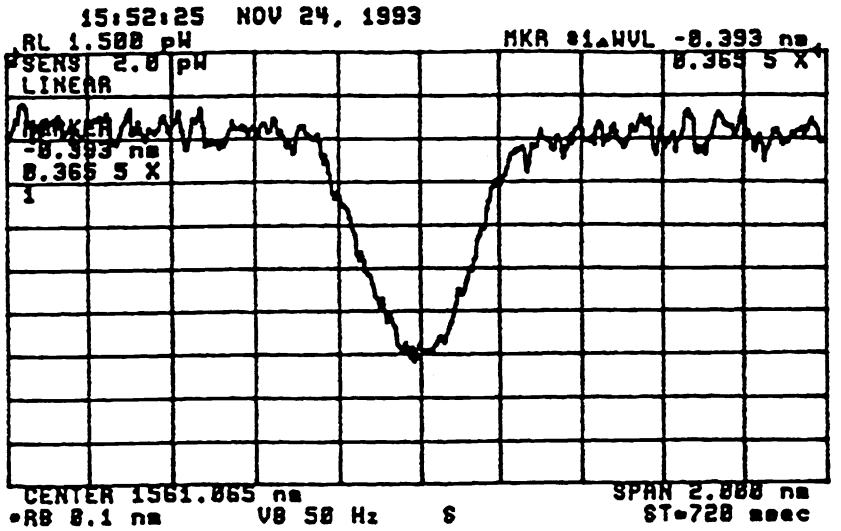

Figure 1. Transmission profile of the grating used.

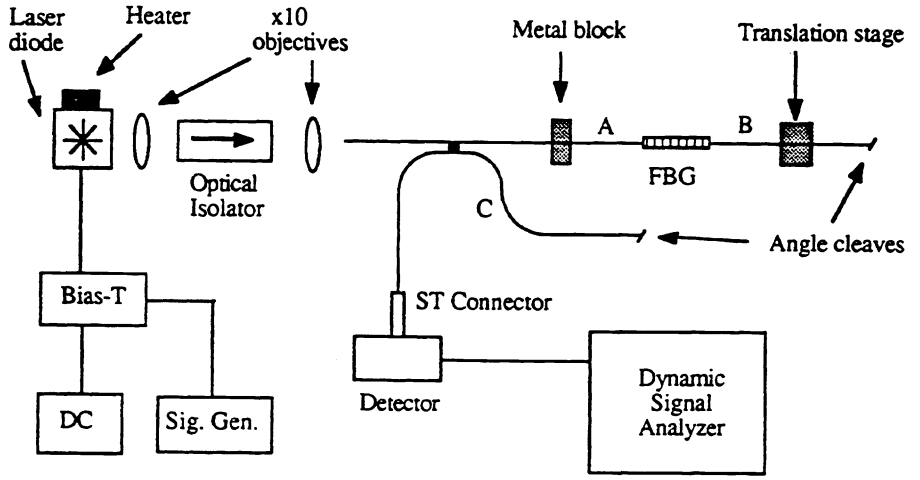

Figure 2. Arrangement used to monitor the second harmonic reflected wavelength.

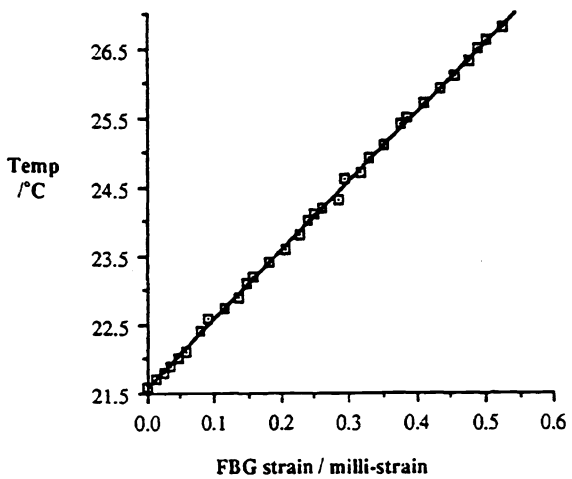

Figure 3. Strain applied to the Bragg grating varying with temperature of the laser diode.

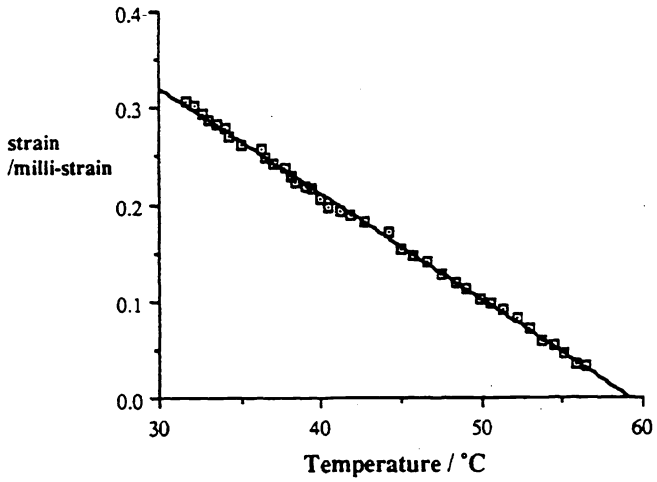

Figure 4. Strain needed to maintain the reflecting wavelength constant as the grating temperature varies.

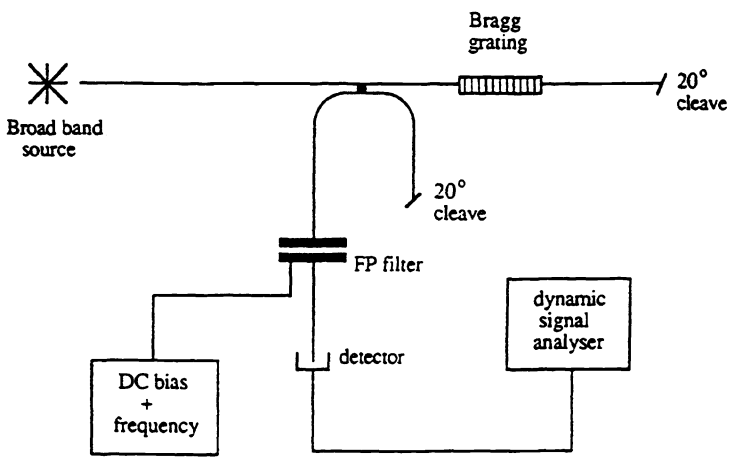

Figure 5. Experimental arrangement for measuring the strain and temperature coefficients at 1561nm.

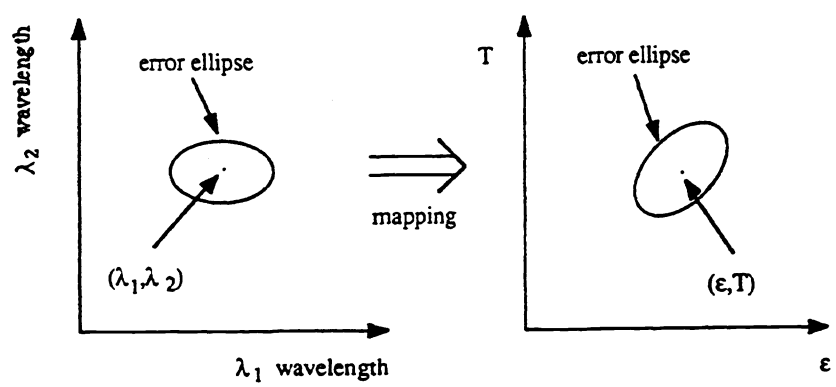

Figure 6. Illustrating the mapping of wavelength space to strain-temperature space.

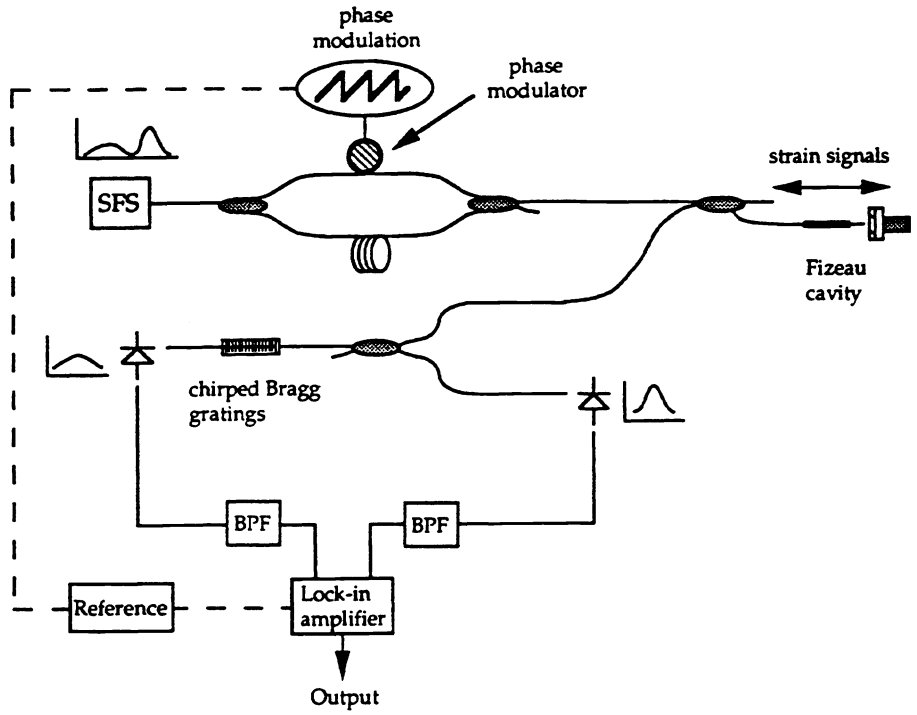

Figure 7. The extended range configuration using a Fizeau cavity coherence tuned to a Mach-Zehnder interferometer and incorporating chirped Bragg gratings to synthesise the dual wavelength output.
SFS - Superfluorescent fibre source. BPF - Band pass filter.

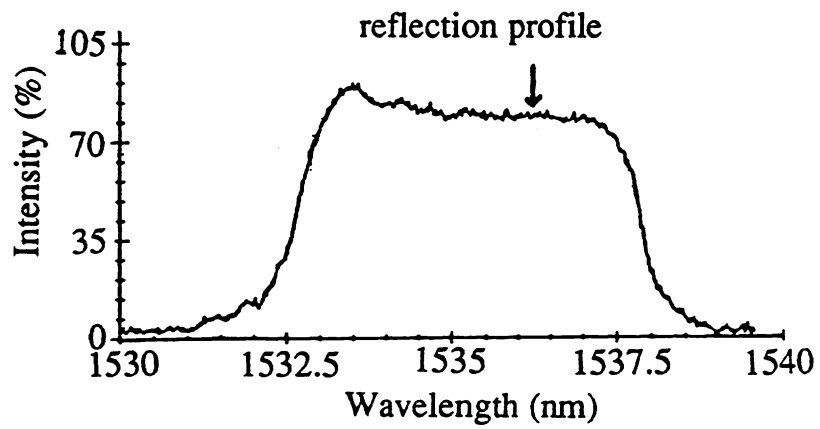

Figure 8. The reflection profile of chirped Bragg grating.

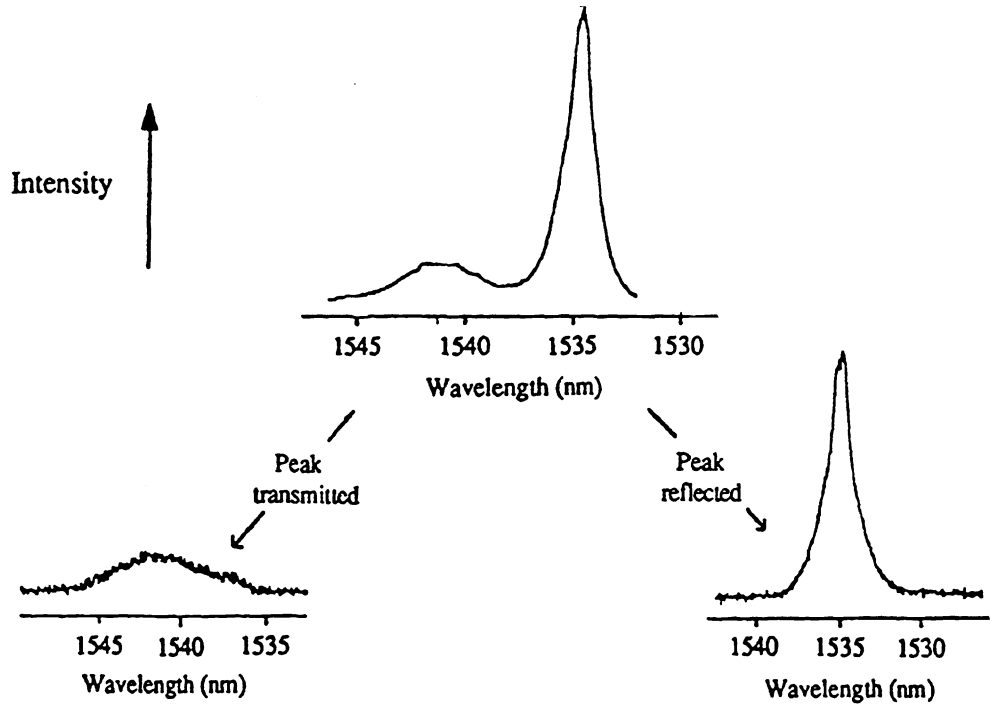

Figure 9. Top trace - the Erbium doped superfluorescent fibre source output incident on the chirped gratings. Bottom trace left - peak transmitted. Bottom trace right - peak reflected.
Vertical scale in arbitrary units.

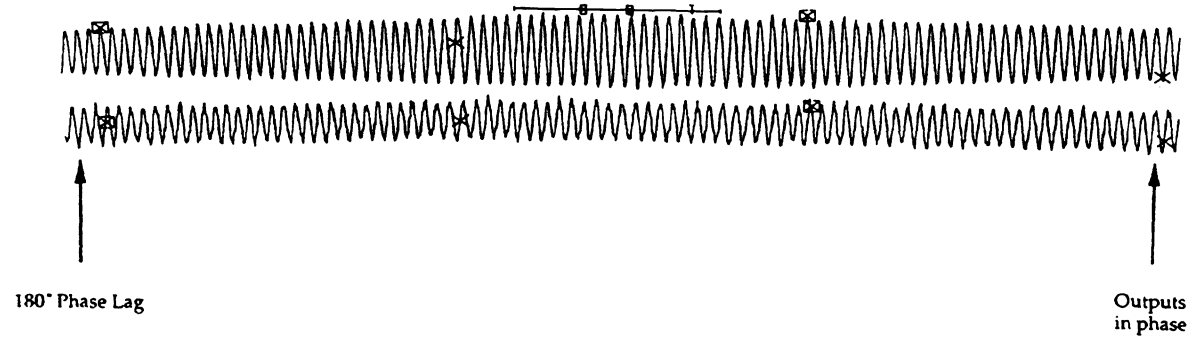

Figure 10. Raw demultiplexed outputs from the dual wavelength Fizeau cavity sensor when subjected to a large linear displacement. Note: a phase ramp was not applied to the Mach-Zehnder interferometer.

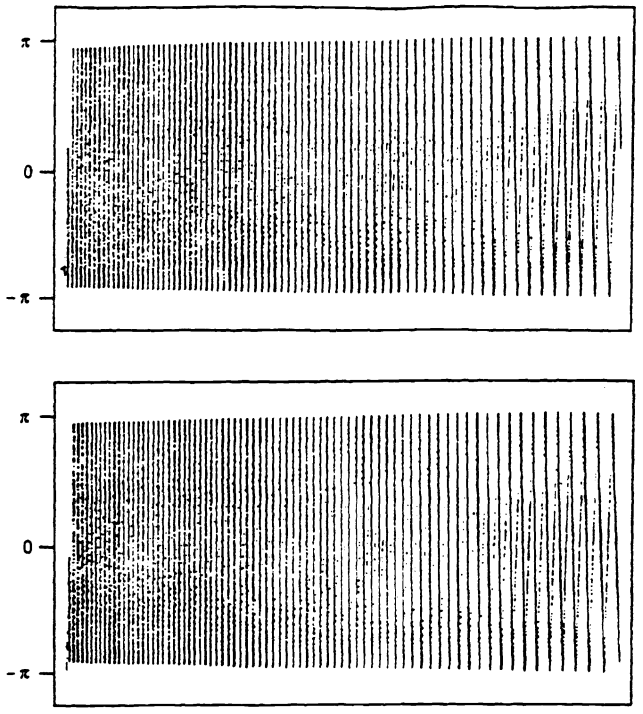

Figure 11. The outputs from the phase comparators monitoring the two single wavelength outputs. Top trace is for λ=1541.4nm and the bottom trace is for λ=1534.8nm.

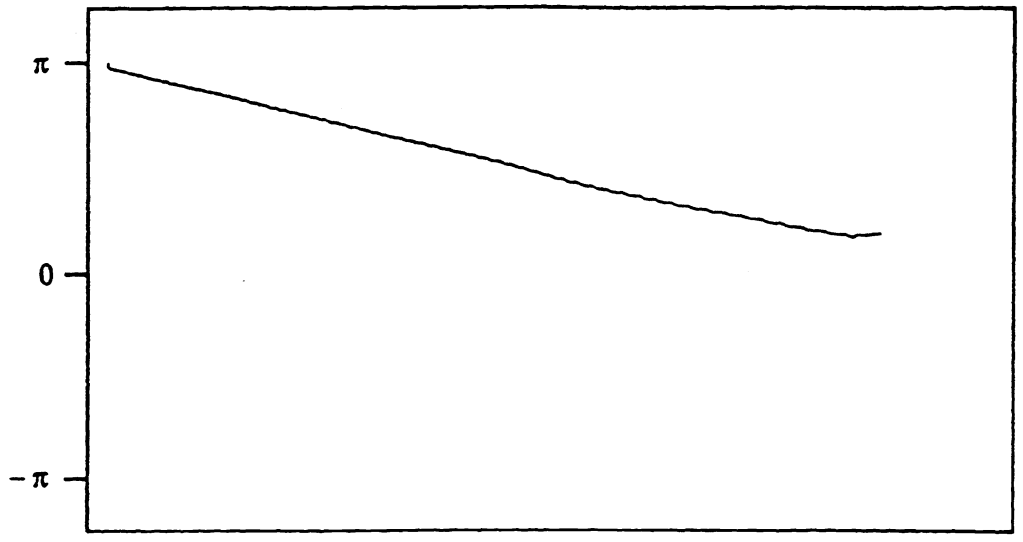

Figure 12. The phase difference of the two wavelengths used to give the extended sensing range.